



## **RESPONSE-SPECTRUM-BASED ESTIMATES OF MOHR'S CIRCLE**

**Charles MENUN<sup>1</sup>**

### **SUMMARY**

The utility of Mohr's circle as an aid for stress analysis is primarily due to its concise graphical nature, which facilitates the identification of the critical combinations of normal and shear stresses acting within a structure. For example, when the capacity of a material is defined by a normal/shear stress interaction diagram, such as the Mohr rupture diagram for reinforced concrete, Mohr's circle can be superimposed on the interaction diagram to identify any combinations of normal and shear stresses that lie in the failure domain of the material. During an earthquake, the radius and center of Mohr's circle naturally fluctuate in time. In such cases, an envelope that bounds the time-varying realizations of Mohr's circle is useful for identifying the critical combinations of normal and shear stresses at that location. In this paper, a response-spectrum-based procedure for predicting the envelope that bounds Mohr's circle in a two- or three-dimensional structure subjected to seismic loads is presented. The implementation and accuracy of the proposed procedure is illustrated for two concrete dams. Comparison of the predicted envelopes with those generated from an ensemble of time-history analyses show that the proposed envelope has a level of accuracy that is commensurate with its response spectrum bases and is suitable for structural analysis and design.

### **INTRODUCTION**

The state of stress at any location within a three-dimensional structure can be quantified by its 3×3 stress tensor, whose elements represent the normal and shear stresses that act parallel and perpendicular to the faces of an infinitesimal cube. The admissible combinations of normal and shear stresses acting on an oblique plane cut through the cube can be summarized by using the information provided by the stress tensor to plot Mohr's circle. The utility of Mohr's circle as an aid for stress analysis is primarily due to its concise graphical nature, which facilitates the identification of the critical combinations of normal and shear stresses. For example, when the capacity of the material is defined by a normal/shear stress interaction diagram, such as the Mohr rupture diagram for reinforced concrete (see, e.g., Mehta [1]), Mohr's circle can be superimposed on the interaction diagram to identify any combinations of normal and shear stresses that lie in the failure domain of the material.

Procedures for plotting Mohr's circle are described in many textbooks that cover advanced topics in mechanics of materials. Naturally, however, when a structure is subjected to seismic loads, the size and location of Mohr's circle is a function of time. In such cases, an envelope that bounds all realizations of

---

<sup>1</sup> Assistant Professor, Stanford University. Email: [menun@stanford.edu](mailto:menun@stanford.edu)

Mohr's circle over the duration of the earthquake is a useful design aid. In references [2] and [3] response-spectrum-based procedures for computing the envelope that bounds the time-varying realizations of Mohr's circle were developed. In this paper, we describe the implementation and application of these procedures for the seismic analysis of two- and three-dimensional structures.

The proposed procedure is based on the response spectrum method and the Penzien-Watabe characterization of multi-component ground motions [4]. Consequently, it inherits the assumptions and approximations implicit in these idealizations, which naturally affect the accuracy of the envelope. We examine the accuracy of the proposed envelope by comparing it to simulated envelopes obtained from an ensemble of time-history analyses performed on two concrete dams. These numerical examples serve to demonstrate that the procedure has a level of accuracy that is commensurate with its response spectrum basis and suitable for structural design and analysis. We also demonstrate how the proposed envelope may be used in conjunction with a prescribed interaction diagram for the purposes of assessing the seismic safety of a structure.

### MOHR'S CIRCLE FOR STATIC STATES OF STRESS

We assume that the geometry of the structure being analysed is defined with respect to a global  $z_1$ - $z_2$ - $z_3$  coordinate system in which the  $z_1$  and  $z_2$  axes lie in the horizontal plane and the  $z_3$  axis is vertical. The state of stress at any location of interest within the structure is defined by the symmetric stress tensor

$$\boldsymbol{\sigma} = \begin{bmatrix} \sigma_{11} & \sigma_{12} & \sigma_{13} \\ \sigma_{21} & \sigma_{22} & \sigma_{23} \\ \sigma_{31} & \sigma_{32} & \sigma_{33} \end{bmatrix}. \quad (1)$$

As indicated in Figure 1a, the diagonal elements of the tensor are the normal stresses acting on an infinitesimal element at the location of interest, while the off-diagonal terms are the shear stresses.

Now consider a second set of orthogonal axes,  $z'_1, z'_2$  and  $z'_3$ , that are rotated with respect to the global coordinate system by means of the transformation  $\mathbf{z}' = \mathbf{A}\mathbf{z}$ , where  $\mathbf{z} = [z_1, z_2, z_3]^T$ ,  $\mathbf{z}' = [z'_1, z'_2, z'_3]^T$  and  $\mathbf{A}$  is the  $3 \times 3$  rotational transformation matrix

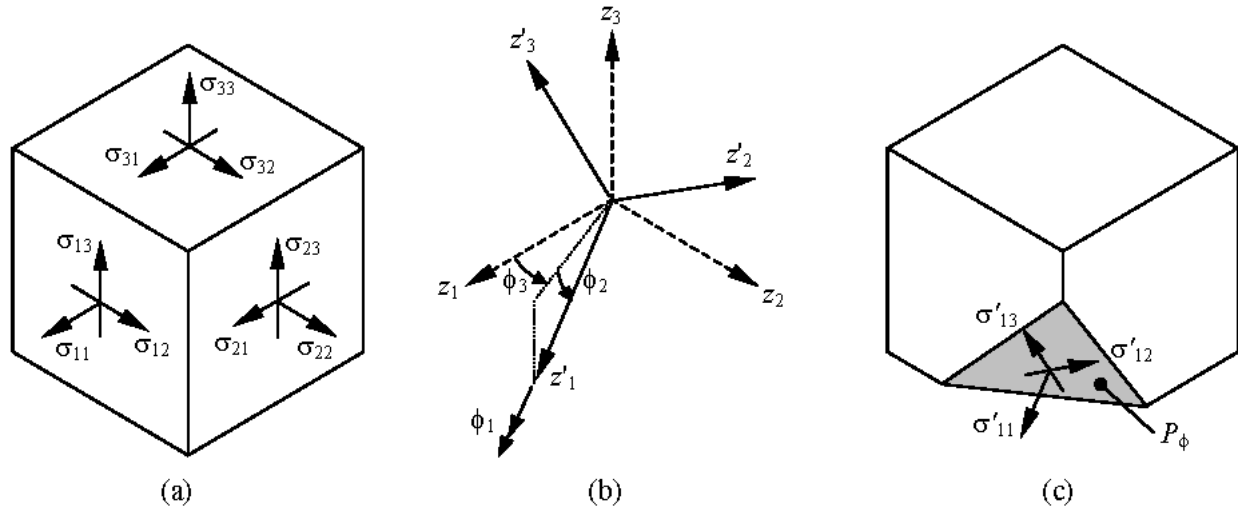


**Figure 1. Normal and shear stresses acting on an infinitesimal element and on an oblique plane defined by rotations  $\phi_1$ ,  $\phi_2$  and  $\phi_3$  about coordinate axes.**

$$\mathbf{A} = \begin{bmatrix} \cos \phi_2 \cos \phi_3 & \cos \phi_2 \sin \phi_3 & -\sin \phi_2 \\ \sin \phi_1 \sin \phi_2 \cos \phi_3 - \cos \phi_1 \sin \phi_3 & \sin \phi_1 \sin \phi_2 \sin \phi_3 + \cos \phi_1 \cos \phi_3 & \sin \phi_1 \cos \phi_2 \\ \cos \phi_1 \sin \phi_2 \cos \phi_3 + \sin \phi_1 \sin \phi_3 & \cos \phi_1 \sin \phi_2 \sin \phi_3 - \sin \phi_1 \cos \phi_3 & \cos \phi_1 \cos \phi_2 \end{bmatrix}, \quad (2)$$

in which  $\phi_1$ ,  $\phi_2$  and  $\phi_3$  represent counter-clockwise rotations about the  $z_1$ ,  $z_2$  and  $z_3$  axes, respectively. In formulating  $\mathbf{A}$ , it is assumed that rotation  $\phi_3$  about the  $z_3$  axis is applied first followed by rotations about the resulting  $z_2$  and  $z_1$  axes, in that order, as indicated in Figure 1b. According to the theory of stress transformations (see, e.g., [5], pp. 21-27), the stress tensor  $\boldsymbol{\sigma}'$  associated with the normal and shear stresses acting parallel and perpendicular to the rotated  $\mathbf{z}'$  coordinate system is related to  $\boldsymbol{\sigma}$  through the transformation

$$\boldsymbol{\sigma}' = \mathbf{A} \boldsymbol{\sigma} \mathbf{A}^T. \quad (3)$$

As indicated in Figure 1c,  $\sigma'_{11}$  obtained from (3) is the normal stress acting perpendicular to the oblique plane  $P_\phi$  whose outward normal is the  $z'_1$  axis. Similarly, the shear stresses acting on  $P_\phi$  in the directions parallel to the  $z'_2$  and  $z'_3$  axes are  $\sigma'_{12}$  and  $\sigma'_{13}$ , respectively.

It is well known that the eigenvalues of  $\boldsymbol{\sigma}$ , which we denote  $\sigma^*_{11} \geq \sigma^*_{22} \geq \sigma^*_{33}$ , are the principal stresses acting at the location of interest and the directions in which they act are the corresponding eigenvectors. Each pair of principal stresses can be used to construct Mohr's circle associated with a rotation of the infinitesimal element about the axis (eigenvector) corresponding to the other principal stress, as indicated in Figure 2. Note that the largest of these circles, associated with  $\sigma^*_{11}$  and  $\sigma^*_{33}$  acts as an upper bound on the possible combinations of normal and shear stresses that the element can experience; thus, we focus our attention on Mohr's circle defined by  $\sigma^*_{11}$  and  $\sigma^*_{33}$ . While the procedure suggested by Figure 2 for plotting this circle is straightforward, it is impossible to implement in the context of the response spectrum method. An alternative method of computing the coordinates of Mohr's circle, which can be incorporated into a response-spectrum-based approach, is described in reference [3] and summarized below.

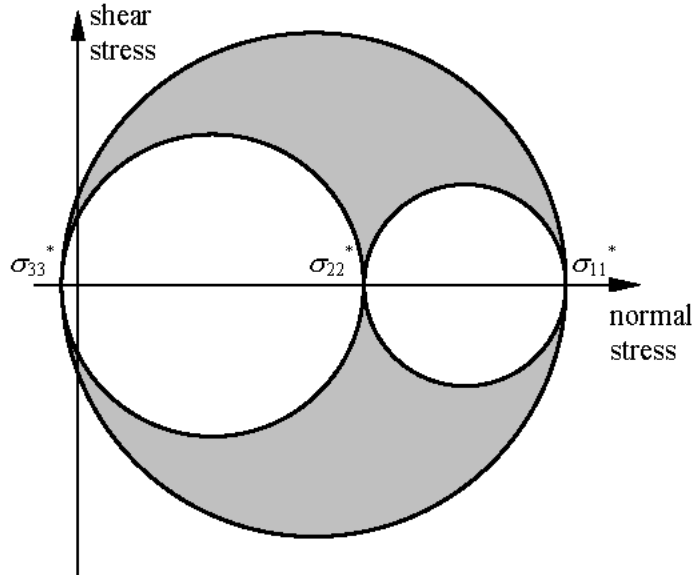


**Figure 2. Mohr's circles for a three-dimensional state of stress.**

First, let the  $6 \times 1$  vector,  $\mathbf{s}_0 = [s_{10}, s_{20}, \dots, s_{60}]^T = [\sigma_{11}, \sigma_{22}, \sigma_{33}, \sigma_{12}, \sigma_{23}, \sigma_{13}]^T$  represent the static state of stress at the location of interest. Upon expanding (3) and rearranging the resulting terms to suit this vectorial representation of the stresses, we can write

$$\sigma'_{11} = \sum_{q=1}^6 T_{q1} s_{qO} \quad (4a)$$

and

$$\sigma'_{13} = \sum_{q=1}^6 T_{q2} s_{qO} , \quad (4b)$$

where  $T_{qi}$  is the trigonometric function in the  $q$ th row and  $i$ th column of the  $6 \times 2$  transformation matrix

$$\mathbf{T} = \begin{bmatrix} \cos^2 \phi_2 \cos^2 \phi_3 & \cos \phi_2 \cos \phi_3 (\cos \phi_1 \sin \phi_2 \cos \phi_3 + \sin \phi_1 \sin \phi_3) \\ \cos^2 \phi_2 \sin^2 \phi_3 & \cos \phi_2 \sin \phi_3 (\cos \phi_1 \sin \phi_2 \sin \phi_3 - \sin \phi_1 \cos \phi_3) \\ \sin^2 \phi_2 & -(\cos \phi_1 \sin 2\phi_2) / 2 \\ \cos^2 \phi_2 \sin 2\phi_3 & -\sin \phi_1 \cos \phi_2 \cos 2\phi_3 + (\cos \phi_1 \sin 2\phi_2 \sin 2\phi_3) / 2 \\ -\sin 2\phi_2 \sin \phi_3 & \cos \phi_1 \cos 2\phi_2 \sin \phi_3 + \sin \phi_1 \sin \phi_2 \cos \phi_3 \\ -\sin 2\phi_2 \cos \phi_3 & \cos \phi_1 \cos 2\phi_2 \cos \phi_3 - \sin \phi_1 \sin \phi_2 \sin \phi_3 \end{bmatrix} . \quad (5)$$

It is shown in reference [3] that each point on Mohr's circle corresponds to a unit direction vector  $\boldsymbol{\alpha} = [\cos \psi, \sin \psi]^T$  in the  $\sigma'_{11} - \sigma'_{13}$  plane defined by a counter-clockwise angle  $\psi$  measured from the  $\sigma'_{11}$  axis and a unique combination of rotations  $\phi_1$ ,  $\phi_2$  and  $\phi_3$  that maximizes

$$M_\alpha = \boldsymbol{\alpha}^T \mathbf{s}'_O = \sum_{q=1}^6 (T_{q1} \cos \psi + T_{q2} \sin \psi) s_{qO} , \quad (6)$$

which is simply the projection of the stress vector,  $\mathbf{s}'_O = [\sigma'_{11}, \sigma'_{13}]^T$  on to  $\boldsymbol{\alpha}$ . Thus, the largest Mohr's circle in Figure 2 can be generated by specifying a number of directions  $0 \leq \psi \leq 2\pi$  in the  $\sigma'_{11} - \sigma'_{13}$  plane and, for each direction, plotting  $\sigma'_{11}$  and  $\sigma'_{13}$  (computed using (4a) and (4b)) that correspond to the combination of  $\phi_1$ ,  $\phi_2$  and  $\phi_3$  that maximizes (6). While this approach is computationally cumbersome compared to conventional procedures used to plot Mohr's circle, it has the advantage that (6) is a linear combination of the normal and shear stresses acting at the location of interest, which is necessary for incorporation into a response-spectrum-based analysis. The nonlinear equations commonly used to compute Mohr's circle are not compatible with the response spectrum method.

We remark that the above procedure can be easily specialized for the case of plane stress or plane strain in two-dimensional structures by setting rotations  $\phi_1 = \phi_3 = 0$ . In this case, the terms in rows 2, 4 and 5 of the transformation matrix  $\mathbf{T}$  are zero and the corresponding stresses,  $s_{2O} = \sigma_{22}$ ,  $s_{4O} = \sigma_{12}$  and  $s_{5O} = \sigma_{23}$  are inconsequential to the analyses. Naturally, only the value of  $\phi_2$  that maximizes (6) must be determined for each direction  $\psi$  considered when plotting Mohr's circle for the two-dimensional case.

## RESPONSE-SPECTRUM-BASED ENVELOPE FOR MOHR'S CIRCLE

During an earthquake, the state of stress at any location within a structure varies in time. Consequently, the location and size of Mohr's circle also fluctuate. In this section, we summarize a response-spectrum-based procedure for computing the envelope  $E_{Mohr}$  that bounds Mohr's circle as it evolves in time during an earthquake. A detailed derivation and discussion of the procedure can be found in references [2,3].

### Preliminaries

We assume that the structure is linear and classically damped with  $N$  degrees of freedom and that its modal properties are available for the  $n \leq N$  significant modes of vibration. For the  $i$ th mode, let  $\omega_i$  = the natural period,  $\zeta_i$  = the damping ratio and  $\phi_i$  = the mode shape. The mass matrix of the structure model is denoted  $\mathbf{M}$ . We also assume that the influence vectors,  $t_1$ ,  $t_2$  and  $t_3$ , which represent the displacements of

the masses resulting for the static application of a unit ground displacement in the  $z_1$ ,  $z_2$  and  $z_3$  directions, respectively, are available so that the inertia force distribution vectors

$$\mathbf{m}_{ki} = \frac{\boldsymbol{\phi}_i^T \mathbf{M} \mathbf{l}_k}{\boldsymbol{\phi}_i^T \mathbf{M} \boldsymbol{\phi}_i} \mathbf{M} \boldsymbol{\phi}_i \quad (7)$$

may be computed (see Chopra [6], p 483).

The structure is subjected to static loads and seismic ground motions that can act simultaneously in the  $z_1$ ,  $z_2$  and  $z_3$  directions. Each component of ground motion is characterized by its pseudo-acceleration response spectrum. Let  $A_{ki} = A_k(\omega_i, \zeta_i)$  denote the pseudo-acceleration response spectrum ordinate of the  $i$ th mode of vibration for the component of ground motion acting in direction  $z_k$ .

When we apply the force vector  $\mathbf{m}_{ki} A_{ki}$  to the structure, the resulting vector of stresses at any point of interest,  $\mathbf{s}_{ki} = [s_{1ki}, s_{2ki}, \dots, s_{6ki}]^T$  represents the peak earthquake induced stresses associated with the  $i$ th mode of vibration and  $k$ th component of ground motion. The (square of the) response spectrum estimate of the peak value of the  $q$ th stress component,  $S_q = \max |s_q(t)|$  is

$$S_q^2 = \sum_{k=1}^3 \sum_{i=1}^n \sum_{j=1}^n s_{qki} s_{qkj} \rho_{ij}, \quad q = 1, 2, \dots, 6 \quad (8)$$

where  $\rho_{ij}$  is the correlation coefficient associated with the  $i$ th and  $j$ th modal responses (Chopra [6], pp. 516-559). In the following discussion, we also make use of the response-spectrum-based cross term,

$$S_{qr} = \sum_{k=1}^3 \sum_{i=1}^n \sum_{j=1}^n s_{qki} s_{rki} \rho_{ij}, \quad q, r = 1, 2, \dots, 6 \quad (9)$$

which is related to the covariance between the  $q$ th and  $r$ th stress components when  $q \neq r$  (see Menun [7]). Note that  $S_{qr} = S_{rq}$  and  $S_{qq} = S_q^2$ ; i.e., (8) is a special case of (9). It is convenient to collect (9) for all stress pairs to construct the  $6 \times 6$  symmetric response matrix  $\mathbf{S} = [S_{qr}]$ . We remark that (8) and (9) assume that the components of ground motion directed along the  $z_1$ ,  $z_2$  and  $z_3$  axes are uncorrelated; i.e., the principal components of ground motion coincide with the assumed structure axes. Analysis of recorded accelerograms suggest that it is often reasonable to assume the vertical component of ground motion (directed along the  $z_3$  axis) is a principal component; however, the horizontal principal components of ground motion will, in general be rotated with respect to the assumed  $z_1$  and  $z_2$  axes (Penzien [4]). In this case, (8) and (9) must be modified as described in reference [7]. For brevity however, we assume in this paper that the principal components of ground motion are directed along the assumed structure axes.

### Stress envelope on a specified oblique plane

Central to the computation of  $E_{Mohr}$  is the envelope that bounds the stress vector  $\mathbf{s}'(t) = [\sigma'_{11}(t), \sigma'_{13}(t)]^T$  for prescribed values of  $\phi_1$ ,  $\phi_2$  and  $\phi_3$  as it evolves in time. It can be shown [7] that the envelope that bounds  $\mathbf{s}'(t)$ , which we denote  $E_\phi$ , is an ellipse whose location, size and orientation on the  $\sigma'_{11} - \sigma'_{13}$  plane are defined by  $\mathbf{s}'_o$  and the  $2 \times 2$  response matrix  $\mathbf{S}' = \mathbf{T}^T \mathbf{S} \mathbf{T}$ . In particular, as indicated in Figure 3, for a prescribed direction  $\boldsymbol{\alpha} = [\cos \psi, \sin \psi]^T$  in the  $\sigma'_{11} - \sigma'_{13}$  plane, the coordinates  $\mathbf{s}' = [\sigma'_{11}, \sigma'_{13}]^T$  of a point on  $E_\phi$  are

$$\mathbf{s}' = \mathbf{s}'_o + \frac{\mathbf{S}' \boldsymbol{\alpha}}{\sqrt{\boldsymbol{\alpha}^T \mathbf{S}' \boldsymbol{\alpha}}}, \quad (10)$$

which can be expanded as

$$\begin{Bmatrix} s'_1 \\ s'_2 \end{Bmatrix} = \begin{Bmatrix} s'_{1o} \\ s'_{2o} \end{Bmatrix} + \frac{1}{S'_\alpha} \begin{Bmatrix} S'_{11} \cos \psi + S'_{12} \sin \psi \\ S'_{12} \cos \psi + S'_{22} \sin \psi \end{Bmatrix}, \quad (11a)$$

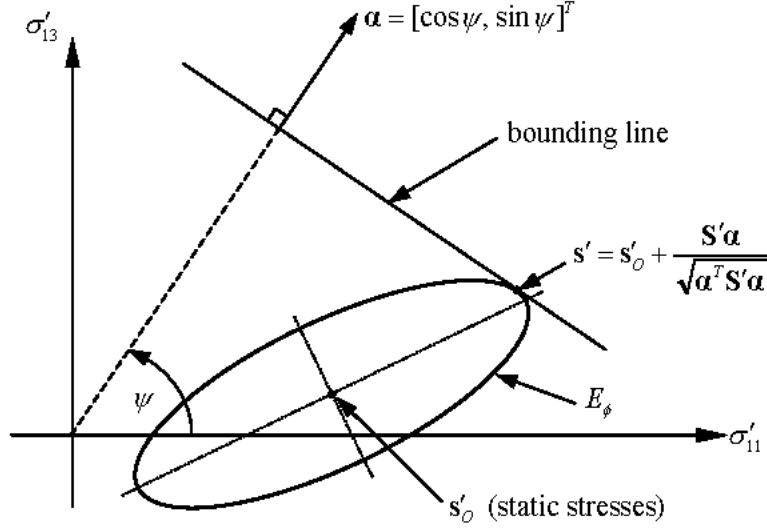


**Figure 3. Elliptical envelope bounding  $s'(t) = [\sigma'_{11}(t), \sigma'_{13}(t)]$ .**

where

$$s'_{iO} = \sum_{q=1}^6 T_{qi} s_{qO}, \quad i=1,2 \quad (11b)$$

$$S'_{ij} = \sum_{q=1}^6 \sum_{r=1}^6 T_{qi} T_{rj} S_{qr}, \quad i, j=1,2 \quad (11c)$$

and

$$\begin{aligned} S'_{\alpha} &= \sqrt{S'_{11} \cos^2 \psi + 2S'_{12} \sin \psi \cos \psi + S'_{22} \sin^2 \psi} \\ &= \sqrt{\sum_{q=1}^6 \sum_{r=1}^6 (T_{q1} \cos \psi + T_{q2} \sin \psi)(T_{r1} \cos \psi + T_{r2} \sin \psi) S_{qr}} \end{aligned} \quad (11d)$$

and we have used the fact that  $S'_{12} = S'_{21}$ . For a prescribed set of rotations,  $\phi_1$ ,  $\phi_2$  and  $\phi_3$ ,  $E_{\phi}$  can be generated by evaluating (11) for a number of closely-spaced values of  $0 \leq \psi \leq 2\pi$  and plotting the resulting  $[s'_1, s'_2]^T = [\sigma'_{11}, \sigma'_{13}]^T$  coordinate pairs.

### Computing $E_{Mohr}$

The procedure for computing the coordinates of the envelope that bounds Mohr's circle in a seismically loaded structure is analogous to that described earlier for the case of static stresses. In particular, we simply replace the static stress vector  $s'_O$  in (6) with  $s'$  defined by (10) and determine the rotations  $\phi_1$ ,  $\phi_2$  and  $\phi_3$  that maximize  $M_{\alpha}$  for a specified direction  $\alpha = [\cos \psi, \sin \psi]^T$  in the  $\sigma'_{11} - \sigma'_{13}$  plane. These optimal values of  $\phi_1$ ,  $\phi_2$  and  $\phi_3$  are then substituted into (11) to determine the coordinates of  $E_{Mohr}$  associated with  $\alpha$ . Repeating this exercise to a number of angles  $0 \leq \psi \leq 2\pi$  and plotting the resulting  $[s'_1, s'_2]^T = [\sigma'_{11}, \sigma'_{13}]^T$  coordinate pairs generates the entire envelope.

When we substitute (10) into (6) and expand, the expression that must be maximized can be written as

$$M_{\alpha} = \sum_{q=1}^6 (T_{q1} \cos \psi + T_{q2} \sin \psi) s_{qO} + \sqrt{\sum_{q=1}^6 \sum_{r=1}^6 (T_{q1} \cos \psi + T_{q2} \sin \psi)(T_{r1} \cos \psi + T_{r2} \sin \psi) S_{qr}}. \quad (12)$$

We remark that the rotations to be determined,  $\phi_1$ ,  $\phi_2$  and  $\phi_3$ , only appear in the evaluation transformation matrix elements  $T_{qi}$  (5). The combination of  $\phi_1$ ,  $\phi_2$  and  $\phi_3$  that maximizes  $M_\alpha$  for a specified value of  $\psi$  must satisfy the set of equations  $dM_\alpha/d\phi_i = 0$ ,  $i = 1, 2, 3$  such that the second derivatives of  $M_\alpha$  with respect to these rotations are less than zero. However, due to the nonlinear nature of (12), this approach is impractical; instead, we suggest that the critical values of  $\phi_1$ ,  $\phi_2$  and  $\phi_3$  be found by systematically evaluating (12) for many uniformly spaced combinations of these rotations and selecting that which maximizes (12). Experience with this “brute-force” approach indicates that it is not computationally prohibitive; e.g., in the numerical examples that follow, only 20 equally spaced values of each rotation in  $[0, \pi]$  were used (i.e.,  $20^3 = 8000$  evaluations of  $M_\alpha$ ), yielding an estimate of  $\max(M_\alpha)$  that is was always within 2% of the true solution. Moreover, we note that the stresses due to static loads,  $s_{q0}$ , and the response spectrum stress cross terms,  $S_{qr}$ , in (12) are not functions of  $\phi_1$ ,  $\phi_2$ ,  $\phi_3$  or  $\psi$ . Consequently, only one structural analysis (needed to compute  $s_{q0}$ ) and one eigenvalue analysis (needed to compute  $S_{qr}$ ) must be performed with respect to the assumed global coordinate system used to define the geometry of the structure, thereby further reducing the computational burden of repeatedly evaluating (12).

Often the analyst is only interested in estimates of the maximum and minimum normal (principal) stresses or the maximum shear stress acting within a structure. These quantities, which coincide with the extreme values of  $E_{Mohr}$  in the  $\sigma'_{11}$  and  $\sigma'_{13}$  directions, respectively, are readily available from the procedure described above for predicting the coordinates of  $E_{Mohr}$ . In particular, it should be apparent that estimates of the maximum and minimum principal stresses are obtained when (12) is maximized with  $\psi = 0$  and  $\psi = \pi$ , respectively. Similarly, the maximum shear stress (and the expected value of the normal stress that acts concurrently) is obtained when  $\psi = \pi/2$  is used.

Recall that  $S_r^2$  and  $S_{qr}$  defined by (8) and (9) assume that the components of ground motion directed along the  $z_1$ ,  $z_2$  and  $z_3$  axes are uncorrelated. If this assumption is not valid and the horizontal principal components of ground motion are rotated with respect to the horizontal  $z_1$  and  $z_2$  axes of the structure model by an (usually unknown) angle  $\theta$ , then  $S_r^2$  and  $S_{qr}$  are functions of  $\theta$ . In this case,  $M_\alpha$  defined by (12) must be maximized with respect to  $\phi_1$ ,  $\phi_2$ ,  $\phi_3$  and  $\theta$ . Fortunately, as shown in reference [3], the optimisation of  $M_\alpha$  with respect to  $\theta$  can be uncoupled from the optimisation with respect to  $\phi_1$ ,  $\phi_2$  and  $\phi_3$  described above, so the additional computational burden introduced by treating  $\theta$  as an unknown quantity is small.

Finally, we remark that the above procedures for predicting the coordinates of  $E_{Mohr}$  or the extreme principal or shear stresses can be easily specialized for the cases of plane stress or plane strain in two-dimensional structures by setting rotations  $\phi_1 = \phi_3 = 0$  and maximizing  $M_\alpha$  defined by (12) with respect to  $\phi_2$  only.

## ACCURACY OF THE PROPOSED ENVELOPE

### Example structures

To test the accuracy of  $E_{Mohr}$ , we compare it to simulated envelopes obtained from a series of time-history analyses performed on the two-dimensional finite element model of a concrete gravity dam shown in Figure 4 and the three-dimensional model of a concrete arch dam shown in Figure 5. All nodes in the finite element models, except those along the bases of the dams and along the abutments of the arch dam, are free to translate. To avoid unnecessarily complicating the following analyses, the foundations are rigid and the reservoirs are empty (i.e., there are no hydrostatic or hydrodynamic forces acting on the upstream faces of the dams). The concrete in the dams is modeled as a homogeneous, isotropic, linear-elastic solid that has modulus of elasticity, Poisson’s ratio and density shown in Figures 4 and 5. Using these material

properties, the global stiffness matrices,  $\mathbf{K}$ , and consistent mass matrices,  $\mathbf{M}$ , of the dams are assembled by standard procedures [8]. Energy is dissipated in the models by viscous damping, which is represented by the damping matrix  $\mathbf{C} = \alpha\mathbf{M} + \beta\mathbf{K}$ , where  $\alpha = 1.6$  and  $\beta = 0.001$  are coefficients chosen such that the resulting modal damping ratios are reasonable for the severity of ground shaking considered.

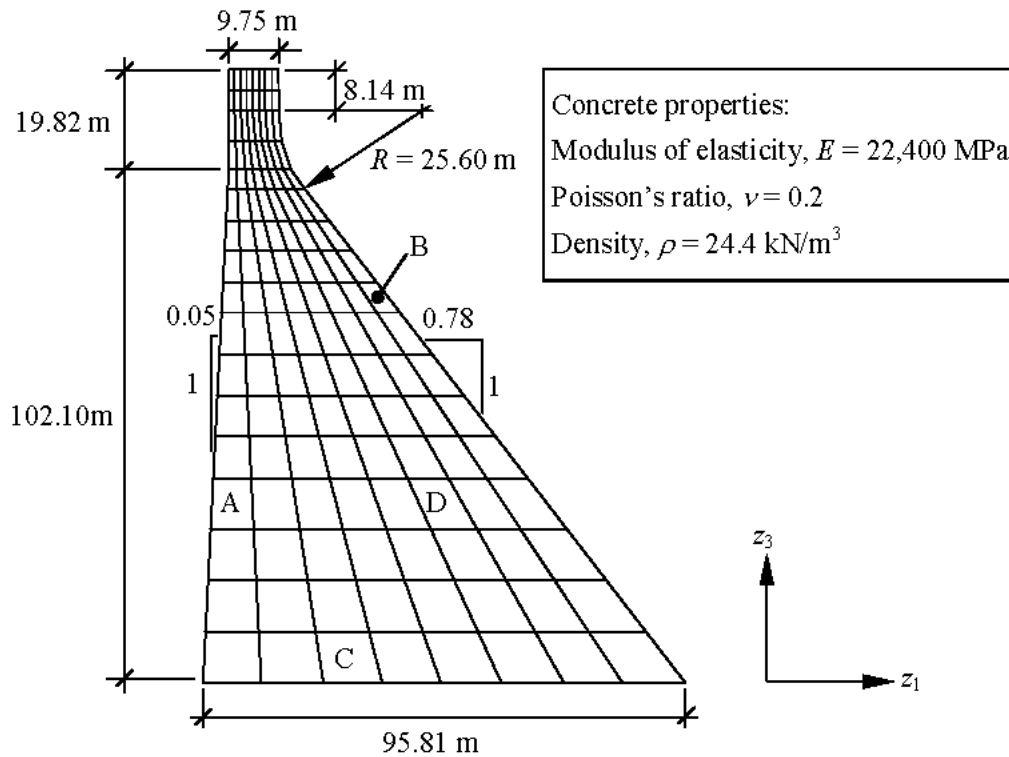


**Figure 4. Finite element model of the example gravity dam.**

### Ground motions

The dams are subjected to ensembles of 20 simulated ground accelerations that were generated in a manner similar to that described in [9], which produces statistically independent realizations of a wide-band, zero-mean Gaussian process. The modulating function used to model the temporal variation of the ground motion intensity was selected such that the resulting accelerograms have a stationary strong motion phase that is several times longer than the fundamental periods of the dams, as assumed by the response spectrum method. The average peak ground accelerations of the major, intermediate and minor principal components of the ground motion are 0.20g, 0.15g and 0.12g, respectively. It is assumed that ground motions of this intensity are representative of a serviceability level earthquake, during which the structures remain elastic and, consequently, the response spectrum method remains valid. A sample accelerogram and its pseudo-acceleration response spectrum, together with the average pseudo-acceleration response spectrum for the major principal component of ground motion are plotted in Figure 6. Owing to the manner in which the ground motions were simulated, the average response spectra of the intermediate and minor principal components have approximately the same spectral shape as the major principal component shown in Figure 6, but with smaller intensities that reflect the fact that these components are not as strong as the major principal component. We remark however that the procedure does not require the components of ground motion have the same spectral shape.



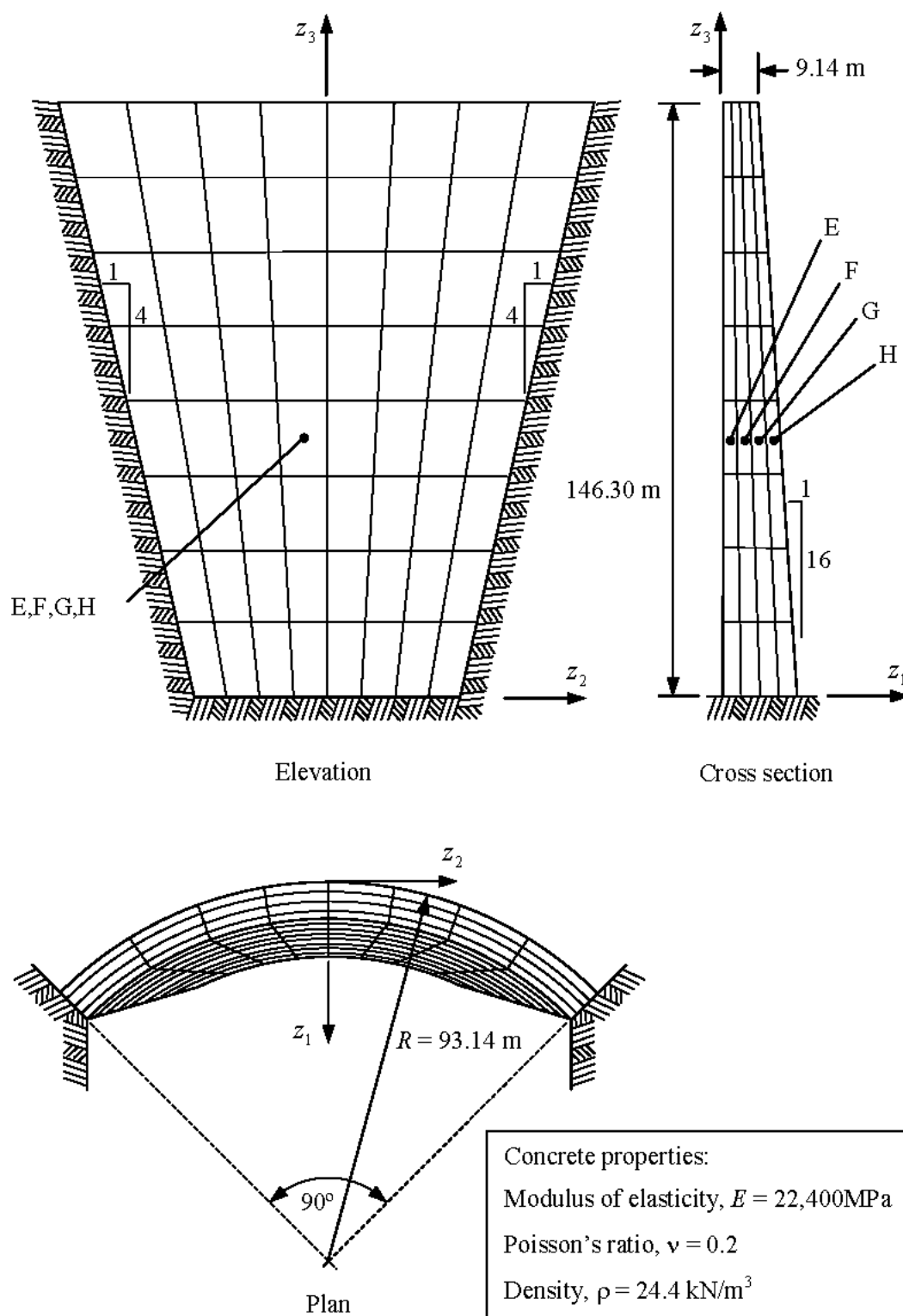
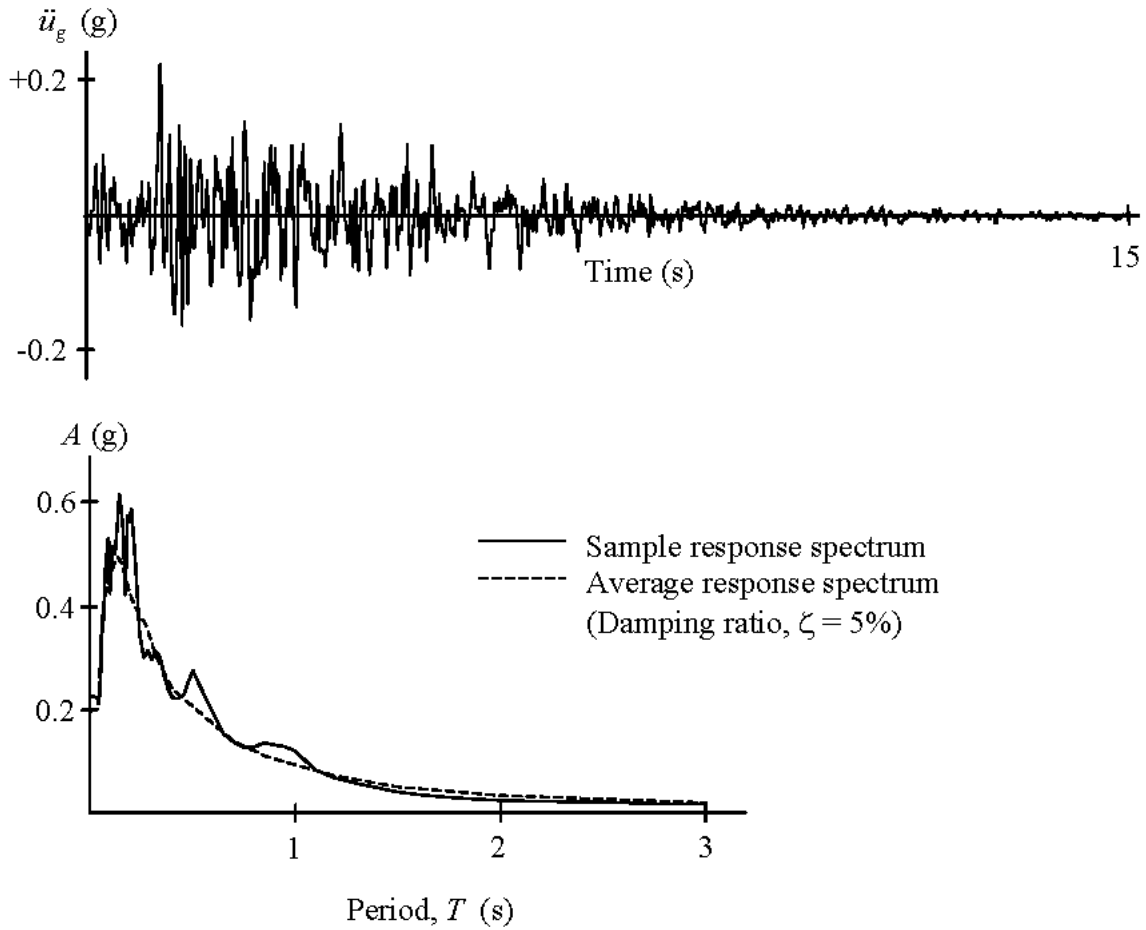


Figure 5. Finite element model of the example arch dam.

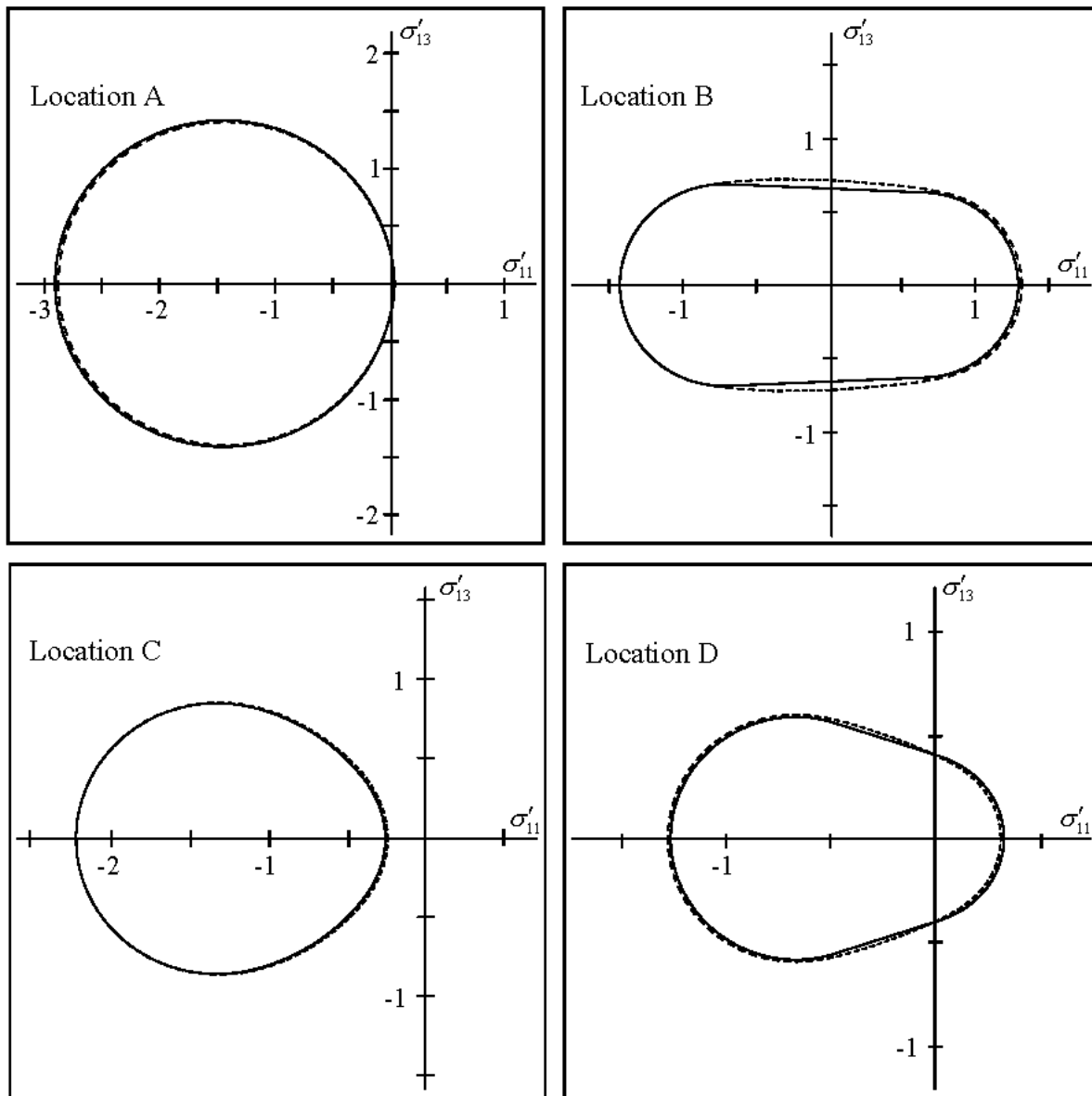


**Figure 6. Sample accelerogram and pseudo-acceleration response spectrum.**

In all time-history analyses, the major principal component of ground motion is directed along the  $z_1$  axis of the structure model, the intermediate principal component is directed along the  $z_2$  axis (for the arch dam only) and the minor principal component is directed along the vertical  $z_3$  axis. For each (principal) component of ground motion, the pseudo-acceleration response spectrum used to evaluate (9) is taken to be the average pseudo-acceleration response spectrum computed for the ensemble of 20 simulated records used for that component in the time-history analyses

#### **Comparison of $E_{Mohr}$ to time-history results**

For each dam, the ensemble of artificial ground motions described above is used to generate 20 realizations of  $s(t)$  at the locations indicated in Figures 4 and 5. These realizations of  $s(t)$  are then used to simulate the average bounding envelope on Mohr's circle (see reference [2] for a description of this calculation), which is compared to  $E_{Mohr}$  computed using the average response spectra of the ground motions. The simulated envelopes at the four locations of interest within each dam are plotted in Figures 7 and 8 along with  $E_{Mohr}$ .



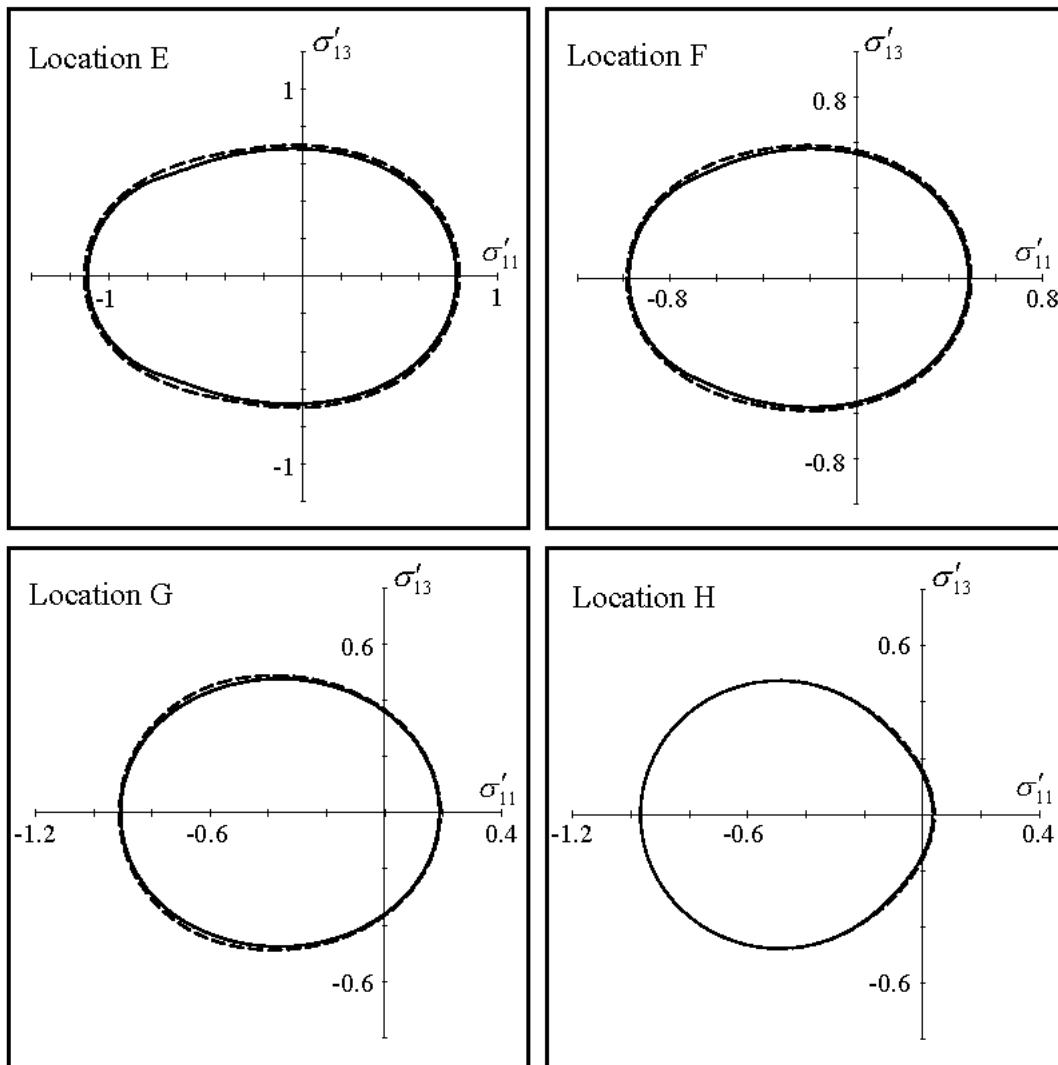
Stresses  $\sigma'_{11}$  and  $\sigma'_{13}$  in MPa. Tensile stresses are positive.

See Figure 4 for locations A, B, C and D.

————  $E_{Mohr}$  computed using the average response spectra of the ensemble of ground motions

----- Simulated mean envelope

**Figure 7.  $E_{Mohr}$  and simulated envelopes bounding Mohr's circle at selected locations in the gravity dam.**



Stresses  $\sigma'_{11}$  and  $\sigma'_{13}$  in MPa. Tensile stresses are positive.

See Figure 5 for locations E, F, G and H.

- $E_{Mohr}$  computed using the average response spectra of the ensemble of ground motions
- Simulated mean envelope

**Figure 8.**  $E_{Mohr}$  and simulated envelopes bounding Mohr's circle at selected locations in the arch dam.

Figures 7 and 8 show excellent agreement between the simulated and predicted envelopes. The largest difference in any direction on the  $\sigma'_{11} - \sigma'_{13}$  plane is less than 10% (along the  $\sigma'_{13}$  axis at location B within the gravity dam) when measured from the origin; however, it is evident that this result is not typical; the discrepancies between the simulated average envelope and  $E_{Mohr}$  are much less in general. The results presented in these figures, which are typical of all locations within the dams, suggest that the proposed envelope is sufficiently accurate for use in structural design and analysis.

### EXAMPLE APPLICATION

We now demonstrate the utility of  $E_{Mohr}$  as an aid to seismic structural analyses by using it to evaluate the adequacy of the concrete in the gravity dam (Figure 4) to withstand all possible combinations of normal and shear stresses that are consistent with the assumed design response spectra of the ground motions (assumed to be the average response spectra of the simulated ground motions plotted in Figure 6). To perform such an assessment at any location of interest within the dam,  $E_{Mohr}$ , which bounds the normal and shear stress demand, must be compared to an appropriate material interaction diagram. In this example, we adopt the Mohr rupture diagram for unreinforced concrete (Mehta [1]) for this purpose. A Mohr rupture diagram is usually determined empirically from a series of triaxial compression tests performed on samples of concrete with increasing confinement pressure. In the following analyses, we assume that the Mohr rupture diagram is a parabola defined by

$$g(\sigma'_{11}, \sigma'_{13}) = f_t \left[ 1 - \left( \frac{\sigma'_{13}}{f_v} \right)^2 \right] - \sigma'_{11} = 0, \quad (13)$$

where  $f_t = 4.8$  MPa and  $f_v = 6.1$  MPa are the nominal tensile and shear strengths of the concrete, respectively. The Mohr rupture diagram defined by (13) is plotted in Figure 9 along with  $E_{Mohr}$  computed at location A in Figure 4.

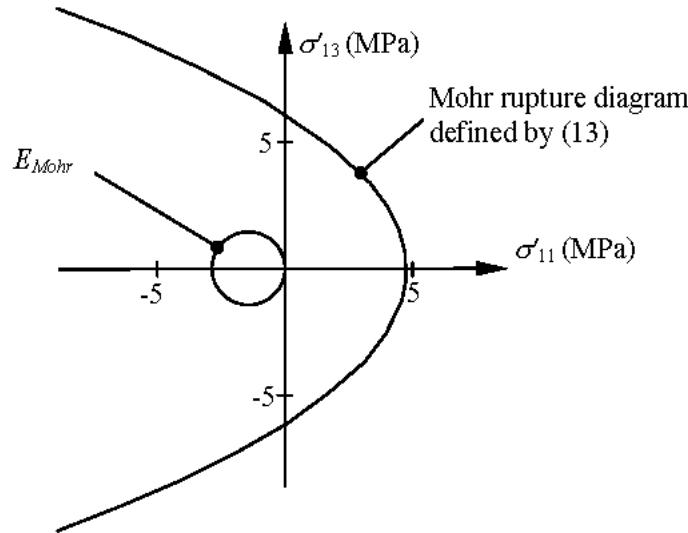
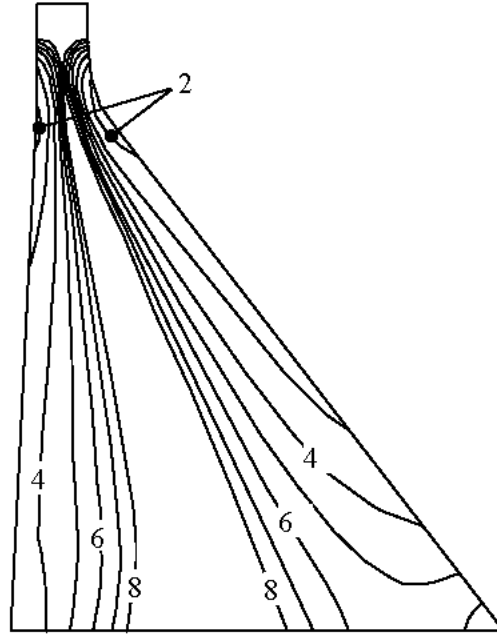


Figure 9.  $E_{Mohr}$  at location A of gravity dam (see Figure 4) and Mohr rupture diagram.

Examining Figure 9, we see that  $E_{Mohr}$  is encompassed by the Mohr rupture diagram, so the concrete is deemed to have adequate strength at this location. Unfortunately, if we wish to examine many locations in the dam, this visual approach is cumbersome to use and an algorithm to automate the analyses is desirable. One such algorithm, which is described in reference [10], operates by computing the required value of a ground motion intensity factor,  $\lambda = \lambda^*$ , that when used to scale the design response spectra used to

evaluate  $S_{qr}$  in (9), causes  $E_{Mohr}$  to expand ( $\lambda > 1$ ) or contract ( $\lambda < 1$ ) such that it touches, but does not cross, the Mohr rupture diagram at one or more points; i.e.,  $\lambda^*$  may be interpreted as a safety factor for the structure. By repeatedly computing  $\lambda^*$  at various locations within the dam, a contour plot, like that shown in Figure 10 can be generated, which upon inspection reveals those critical locations within the dam where the ground motion intensity factor required to cause the concrete to fail is the lowest.



**Figure 10. Contour plots of critical ground motion intensity factor  $\lambda^*$  in gravity dam.**

## CONCLUSIONS

A response-spectrum-based procedure for predicting the envelope,  $E_{Mohr}$ , that bounds Mohr's circle at any location of interest within a two- or three-dimensional structure that is subjected to as many as three translational components of ground acceleration has been described. The envelope is a function of quantities that are routinely used and calculated in conventional response spectrum analyses. When only the extreme normal (principal) or shear stresses are of interest, they can be readily obtained from the envelope; however, it was shown that these stresses can also be computed directly without generating the entire envelope.

For brevity,  $E_{Mohr}$  has been described for the specific case in which the principal (uncorrelated) components of ground motion are directed along the global coordinate axes used to define the structure model. The required modifications for the more general case in which the horizontal principal components of ground motion are rotated with respect to the assumed horizontal axes of the structure model by an unknown angle  $\theta$  can be found in reference [3]. However, these modifications do not significantly change the computation or application of  $E_{Mohr}$  from what is presented in this paper.

The accuracy of the  $E_{Mohr}$  was examined by means of an ensemble of time-history analyses performed on a two-dimension concrete gravity dam and a three-dimensional concrete arch dam using simulated ground motions. The results of these analyses demonstrated that the proposed envelope accurately bounds the

time-varying realizations of Mohr's circle in an average sense. For each of the four locations considered within each dam, the difference between the simulated average envelope and  $E_{Mohr}$  computed using the average response spectra of the ground accelerations was less than 10% in any direction on the normal-shear stress plane measured from the origin. However, it was noted that this discrepancy was not typical; the differences between the simulated and predicted envelopes were much less in general. Thus, we conclude that the proposed envelope is sufficiently accurate for structural analysis and design.

The utility of  $E_{Mohr}$  in structural analysis and design of is similar to that of Mohr's circle for static states of stress. In particular,  $E_{Mohr}$  provides a concise graphical representation of the possible combinations of normal and shear stresses that act at any location of interest within the structure during an earthquake. Consequently, the envelope is a useful design aid, particularly when the capacity of the material is defined by an interaction diagram, as was illustrated for the example gravity dam using a Mohr rupture diagram to represent the capacity of the concrete.

### ACKNOWLEDGMENTS

The author is indebted to Prof. Anil Chopra for suggesting the research described herein and providing thoughtful and encouraging comments during its development. Financial support provided by the US Army Corps of Engineers is also gratefully acknowledged. However, the opinions and conclusions described in the paper are those of the author alone.

### REFERENCES

1. Mehta PK, Monteiro PJM. "Concrete: Structure, Properties and Materials." Second edition. Prentice Hall: Englewood Cliffs, NJ, 1993.
2. Menun C. "A response-spectrum-based envelope for Mohr's circle." Earthquake Engineering and Structural Dynamics 2003; 32:1917-1935.
3. Menun C. "An envelope for Mohr's circle in seismically excited three-dimensional structures." Earthquake Engineering and Structural Dynamics 2004; in press.
4. Penzien J, Watabe M. "Characteristics of three-dimensional earthquake ground motion." Earthquake Engineering and Structural Dynamics 1975; 3:365-374.
5. Ragab A-R, Bayoumi SE. "Engineering Solid Mechanics: Fundamentals and Applications." CRC Press: New York, NY, 1999.
6. Chopra AK. "Dynamics of Structures: Theory and Applications to Earthquake Engineering." Second edition. Prentice-Hall: Upper Saddle River, NJ, 2001.
7. Menun C, Der Kiureghian A. "Envelopes for seismic response vectors. I: Theory." Journal of Structural Engineering ASCE 2000; 126:467-473.
8. Cook RD. "Concepts and Applications of Finite Element Analysis." Second edition. John Wiley and Sons: New York, 1981.
9. Ruiz P, Penzien J. "Probabilistic study of the behavior of structures during earthquakes." Report No. UCB/EERC 69-3, Earthquake Engineering Research Center, University of California, Berkeley, CA, 1969.
10. Menun, C. and Der Kiureghian, A. "Envelopes for Seismic Response Vectors." PEER Report 1999/08, Pacific Earthquake Engineering Center, University of California Berkeley, 1999.